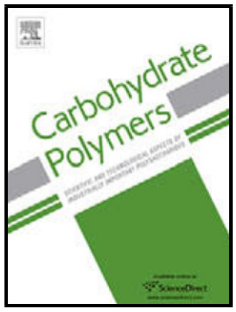

Title: Polyethylenimine/Kappa Carrageenan: Micro-arc Oxidation Coating for Passivation of Magnesium Alloy

Authors: A. Golshirazi, M. Kharaziha, M. Golozar

PII: S0144-8617(17)30280-1
DOI: http://dx.doi.org/doi:10.1016/j.carbpol.2017.03.025
Reference: CARP 12114

To appear in:

Received date: 22-12-2016
Revised date: 2-2-2017
Accepted date: 8-3-2017

Please cite this article as: Golshirazi, A., Kharaziha, M., & Golozar, M., Polyethylenimine/Kappa Carrageenan: Micro-arc Oxidation Coating for Passivation of Magnesium Alloy.*Carbohydrate Polymers* http://dx.doi.org/10.1016/j.carbpol.2017.03.025

Polyethylenimine/Kappa Carrageenan: Micro-arc Oxidation Coating for Passivation of Magnesium Alloy

A. Golshirazi, M. Kharaziha*, M. Golozar

Department of Materials Engineering, Isfahan University of Technology, Isfahan 84156-83111, Iran

- Corresponding author e-mail: ma.kharaziha@gmail.com
- Fax: +93-31-33912752

Highlights

- Micro-arc oxidation and self-assembly approach was applied to reduce corrosion of AZ91
- Silicate-fluoride electrolyte was adopted for MAO treatment
- Polyethylenimine/Kappa Carrageenan coating was applied as the second coating layer.
- Corrosion of MAO-coated AZ91 alloy reduced compared to untreated AZ91
- Double layered PEI/KC:MAO coating presented great resistance to corrosion attack

Abstract

The aim of this study was to combine micro-arc oxidation (MAO) and self-assembly technique to improve corrosion resistivity of AZ91 alloy. While a silicate-fluoride electrolyte was adopted for MAO treatment, polyethylenimine (PEI)/Kappa carrageenan (KC) self-assembly coating was applied as the second coating layer. Resulted demonstrated the formation of forsterite-fluoride containing MAO coating on AZ91 alloy depending on the voltage and time of anodizing process. Addition of the second PEI/KC coating layer on MAO treated sample effectively enhanced the adhesive strength of MAO coated sample due to filling the pores and increase in the mechanical

interlocking of coating to the substrate. Moreover, the corrosion evaluation considered by potentiodynamic polarization and electrochemical impedance spectroscopy confirmed that double layered PEI/KC:MAO coating presented superior resistance to corrosion attack. It is envisioned that the proposed double layered PEI/KC:MAO coating could be useful for biomedical applications.

Keywords: Biodegradable magnesium AZ91; Micro arc oxidation; Self-assembly technique; Kappa Carrageenan; Corrosion resistivity.

1. Introduction

Magnesium (Mg) and its alloys have attracted much interest for biomedical applications due to their biocompatibility, biodegradability, low density (1.74 g cm^{-1}) and high fracture toughness (Xue-Nan GU, 2014). Mg-based implants have provided temporary constructs for tissues such as bone and vessels in order to gradually be dissolved and, finally, be absorbed by the human body. However, Mg-based alloys are known to be greatly reactive and suffering fast electrochemical dissolution in biological environment which results in release of plentiful volumes of hydrogen which are intolerable for body tissues (Agarwal, Curtin, Duffy, & Jaiswal, 2016). Moreover, rapid dissolution of Mg alloys provided high local concentration of Mg^{2+} which may trigger an adverse tissue reaction leading to inadequate *in vivo* bioactivity of Mg-based implants (Gu XN, 2009).

Various strategies consisting of controlling the purity and alloying as well as surface coating and treatment have been introduced as significant approaches to control initial degradation rate (Witte F, 2008; Zeng RC, 2008). Between them, surface treatment approaches such as alkaline heat treatment (X. Gu, Zheng, Cheng, & Zheng, 2009) electrodeposition technique(Li et al., 2010) and anodization treatment (Hiromoto & Yamamoto, 2010) have been widely studied for Mg based alloys. In the last few years, micro-arc oxidation (MAO) is the most commercially protection method for Mg alloys providing an excellent wear and corrosion resistance (A.L. Becker). MAO technique is an electrochemical surface treatment process based on the chemical conversion of the substrate metal into its oxide, and growth both inwards and outwards from the original metal surface. Due to its conversion nature, rather than a deposited coating (such as a coating formed by plasma spraying), MAO technique reveals an excellent adhesion to the substrate metal. Moreover, this technique has the advantages consisting of uncomplicated surface

pretreatment, simple process and low cost and high comprehensive performances such as high wear resistance. Furthermore, the MAO process hardly changes the microstructure and mechanical properties of the treated alloy substrate (Foerst et al., 2013; T.S.N. Sankara Narayanan 2014). However, MAO coatings on Mg alloys consist of micropores and cracks, which could influence the protection performance of the coatings and accelerate the corrosion rate (Dima C.). To further improve the protective properties of MAO coating on Mg alloys, there would be of great significance to remedy the surface defects of MAO coating with various secondary coatings. In this way, wide researches have focused on the deposition of various ceramics and polymers on different Mg alloys (Fan et al., 2014; Xiong, Lu, Wang, & Song, 2015).

In addition to corrosion resistant, other aspects necessary to be addressed for coatings are degradation rate, the ability to release drugs and different growth factors in a controlled manner. Considering all these properties, polymeric coatings reveal remarkably attractive due to the mixture of their chemical and physical characteristics. Furthermore, polymeric coatings could cover the pores of MAO coatings deposited on Mg alloys which reduce corrosion rate (Feliu & Llorente, 2015; R. Dhamodharan, 1999). Recently, enormous progress has been performed in order to self-assemble various polymers into functional materials. Between various assembling techniques, layer-by-layer (LbL) self-assembly approach has attracted significant consideration, especially for biomedical applications (C., 2008; Crouzier T, 2010). LBL approach is based on the alternating deposition of oppositely charged polyelectrolytes in order to develop various multilayered biomedical coatings and films with control thickness on the nanometer scale (Detzel CJ, 2011; Larkin AL, 2010). LBL self-assembly technique has recently been employed to develop anticorrosion coatings on metal surfaces to block the corrosion processes(Madona Lien Paul, 2014; Rodrigo M. Iost, 2012). Polyelectrolytes are classified according to their origin to the synthetic polyelectrolytes (i.e. poly(ethylenimine) (PEI) (A.M. Mansouri & M. Pirsaheb, 2014; Anna Trybała, 2009), poly(styrene sulfonate) (PSS), poly(acrylic acid) (PAA)) (P. Bertrand, 2000) and natural ones (i.e. nucleic acids(A.L. Becker, 2010) and polysaccharides (K. Cai, 2005) such as chondroitin sulfate (R. Dhamodharan, 1999), chitosan (Shu Y, 2011)and kappa carrageenan (KC) (Ana C. Pinheiro, 2012)). Between these polyelectrolytes, PEI has been widely applied in order to develop LbL self-assembly constructs (A.M. Mansouri & M. Pirsaheb, 2014; Syed, Lu, Tang, & Meng, 2015). PEI as an insulating polymer exhibits good

adhesion to substrates that assists in molecular electrostatic self-assembly for the multilayer formation and provides an effective blockage against corrosion without any other inhibiting species(Syed et al., 2015). For instance, Syed *et al.* (Syed et al., 2015) prepared multilayered polyaniline (PANI)-PAA/PEI coatings for corrosion protection of 316 stainless steels by an alternate deposition. They revealed that the combination of PANI-PAA composite with PEI and their multilayer structure provides a synergistic enhancement of corrosion resistance properties. In another words, KC is a sulphated anionic polysaccharide extracted from certain red seaweeds which has been widely applied in food industry as gelling and stabilizing agent (Park, 2001) Recently, nanolayered coating composed of KC and chitosan was developed as a coating to support foods such as fruit, vegetables or cheese (Ferreira, Alves, & Coelhoso, 2016). In another study, LBL coating of KC and chitosan onto a substrate (polyethylene terephthalate) was used as a drug delivery system (Ana C. Pinheiro, 2012). According to our knowledge, KC has not been evaluated for LBL coatings on Mg based alloys.

The aim of this study was to combine MAO technique and LbL self-assembly approach to improve the corrosion resistance of AZ91 magnesium alloy. PEI and KC were chosen as the polyanion and polycation for the LbL self-assembly system, respectively. In this regard, after optimization of MAO coating approach based on the coating thickness and electrochemical properties, PEI and KC were coated, subsequently. Finally, the structural, chemical, electrochemical and physical properties of coated samples were evaluated. It is expected that combined MAO-LBL coating could significantly improve the corrosion resistance of AZ91 alloy, which could be beneficial for biomedical application.

2. Materials and methods

2.1. Sample preparation

AZ91 magnesium alloy specimens with the chemical composition of 8.63 wt.% Al, 0.59 wt.% Zn, 0.17 wt.%, Mn, < 0.05 wt.% Cu, <0.05 wt.% Fe and the balanced Mg were used in the present study. Prior to the MAO treatment, the samples cut into specimens of 20 × 10× 3 mm^3, were polished with various grades SiC abrasive papers (80, 600, 1200 and 2400). Finally, the samples were degreased ultrasonically in acetone for 10 min, rinsed in deionized (DI) water for 30 s and then dried in air.

2.2. Preparation of MAO coating

Before MAO coating process, an aqueous solution of NaOH (100 g/l), Na_2SiO_3 (100g/l) and NaF (20 g/l) (Sigma) was prepared as the electrolyte. A DC power supply (IPC-SL20200J, 20 A, 200 V, Iran) was used for MAO coating. The samples were electrolytically processed at two different voltages (45V and 60 V), for different times (30 and 60 min). According to the working voltage and time, the samples were named as 45v30m, 45v60m, 60v30m and 60v60m, respectively. Initial temperature of the electrolyte was set at 25 °C. In this regard, AZ91 samples were taken as anodes (working electrode) and stainless steel 316L sample was introduced as cathode (counter electrode). The distance between the working and counter electrodes was set to 30 mm. After micro-arc oxidation treatment, the samples were cleaned in DI water and air-dried.

2.3. *Preparation of PEI/KC self-assembled coating*

Primarily, 0.5 gr PEI (Mw ~25,000, 50 wt. % in H_2O, Sigma) solution in 0.14 M NaCl mixture (pH=10) was prepared under magnetic stirring for 10 min. Separately, 2 mg/ml KC (sulfated plant polysaccharide, Sigma) solution in DI water was also prepared under magnetic stirring for 30 min at 100 °C. Anodized AZ91 specimens were immersed in PEI solution for 24 h to obtain an stable positive charge on the surface. After rinsing in DI water and air-drying, PEI coated substrates were dip coated in KC solution and kept for 10 min. Finally, the samples were rinsed with DI water and air-dried. Similarly, PEI/KC coating was also performed on the untreated AZ91 alloy following the procedure used for MAO treated AZ91 substrates.

2.4. Characterization of surface modified samples

The surface and cross-section morphologies of the samples were investigated by scanning electron microscopy (SEM, S360, Cambridge). Before imaging, the samples were sputter-coated with a thin layer of gold and the SEM images along with NIH Image J software were applied to estimate the pore size of the surface samples. The phase constituents of the MAO coating was examined by a X-ray diffractometer (XRD, Philips X'Pert-MPD system) using monochromatized CuKα radiation. The XRD pattern was analyzed with X' Pert software. Moreover, Fourier transform infrared spectroscopy (FTIR, Bomem, MB-100), in the range 600–4000 cm^{-1}, was also applied to determine chemical compositions of the MAO-LBL coatings. The surface roughness (Ra) of the samples, before and after coatings, was measured using a roughness tester (Taylor-Hobson Surtronic Duo, Leicester, England) with a cut-off 5 mm. Three different measurements were collected and the mean roughness value (Ra) and standard deviation were reported, accordingly. Moreover, the adhesion strength of the coatings was

evaluated using epoxy resin (Uhu Epoxy ultra strong, Germany). The samples (n=3) were precoated with epoxy resin with an adhesive strength up to 30 MPa. After curing the epoxy at room temperature for 24 h, tensile tester (Hounsfield H25KS) with loading rate of 0.2 mm/min was applied until the coating layer failed. Finally, the adhesion strength was determined from the maximum load divided by the contact area.

2.5. Evaluation of electrochemical corrosion behavior

The corrosion behavior of the samples was evaluated using potentiodynamic polarization and electrochemical impedance spectroscopy (EIS) in buffer phosphate saline (PBS) at pH= 7.4 and 25± 0.5 °C. A three-electrode electrochemical cell set up consisted of the samples as the working electrodes, Ag/AgCl saturated in potassium chloride (KCl) as the reference electrode and a platinum sheet as the counter electrode was applied. Before potentiodynamic polarization, the samples were immersed in PBS solution for 2 h, in order to reach a quasi-steady state at the electrode/solution interface. The potentiodynamic polarization study was performed in a potential range of ±250 mV vs. open circuit potential (OCP) at the scan rate of 1 mV/s by using AMETEK potentiostat/galvanostat (PARSTAT 2273). For EIS measurement (Potentio mode (PEIS) was applied, the AC signal amplitude was 10 mV and the frequency range was from 10^5 Hz to 10^{-3} Hz. The results of the corrosion tests (E_{corr} and $I_{corr,}$) were estimated by extrapolating the polarization curve based on ASTM-G102-89. In this regard, the corrosion rate (CR) was calculated from cyclic potentiodynamic curves using Tafel extrapolation techniques in accordance with ASTM G-102.

3. Results and discussion

3.1. Characterization of MAO-treated samples

Fig. 1(a) illustrates the XRD patterns of pristine AZ91 as well as MAO-coated AZ91 samples. Pristine AZ91 composed of Mg and $Al_{12}Mg_{17}$ peaks which were the characteristic phases of AZ91 alloy (Rojaee, Fathi, & Raeissi, 2013). After MAO coating, in addition to Mg and MgO (periclase, ICSD code: 01-087-0651), Mg_2SiO_4 (forsterite, ICSD code:01-080-0783) and MgF_2 (ICSD code: 00-038-0882) could be detected depending on the applied voltage and time of MAO process. For instance, XRD pattern of 60v30m sample mainly composed of Mg_2SiO_4, followed by MgO and MgF_2 confirming the engagement of Mg, Si, F and O elements in chemical reactions during MAO process. However, the comparative intensities of ceramic based component diffraction peaks to that of Mg ones were intensified with increasing the

voltage and time of MAO process revealing the formation of thicker coating. MgO and Mg_2SiO_4 components were the comment products of MAO process of magnesium alloys (Durdu, Aytac, & Usta, 2011; Xue, Yun, Schulz, & Shanov, 2011).

During the MAO process, a large number of small-size sparks were generated, randomly distributed and quickly moved over the entire anode (AZ91 alloy) surface. At this condition, the localized high temperature and pressure were produced leading to the formation of discharge channels between the magnesium alloys served as the localized anode and the electrolyte assisted as the localized cathode. In this regard, similar to other conventional MAO process, MgO layer was formed from the collision of $Mg^{2+}$and O^{2-} by outward migration of Mg^{2+} from the metallic substrate via anodic dissolution and inward migration of oxidized O^{2-} from electrolyte to the discharge channels according to the following reaction (reaction 1)(Guo, An, Huo, Xu, & Wu, 2006):

$$Mg^{2+} + O^{2-} \rightarrow MgO \quad (1)$$

During the penetration of SiO_3^{2-} from electrolyte into the micro discharge channels and its direct oxidation according to reaction 2, SiO_2 was formed on the surface of sample (Xin, Song, Zhao, & Hu, 2006). Hence, due to the localized high temperature and pressure in MAO process, while micro arcs went out, due to the cooling consequence of electrolyte, phase transformation between molten SiO_2 and MgO resulted in the formation of Mg_2SiO_4 phase according to the reaction 3(Gnedenkov et al., 2010)

$$SiO_3^{2-} + 2e^- \rightarrow SiO_2 + 1/2O_2 \quad (2)$$

$$2MgO + SiO_2 \rightarrow Mg_2SiO_4 \quad (3)$$

According to previous research, Mg^{2+} dissolved from the samples in to the electrolyte could also react with SiO_3^{2-} ions leading to the direct formation of Mg_2SiO_4 phase according to reaction 4 (Salih Durdu, 2012).

$$2Mg^{2+} + 2SiO_3^{2-} \rightarrow Mg_2SiO_4 + SiO_2 \quad (4)$$

Moreover, the participation of fluoride ions from the NaF component of electrolyte (reaction 5) during MAO process directed to the formation of MgF_2 phase (reaction 6) along with MgO. This compact MgF_2 passive film acted as a parameter to control the thickness of coating via the prohibition from the excessive anodic dissolution during the initial stages of MAO process (T.S.N. Sankara Narayanan 2014).

$NaF \rightarrow Na^{+} + F^{-}$ (5)

$Mg^{2+} + 2F^{-} \rightarrow MgF_2$ (6)

SEM images of pristine and MAO coated samples provided at various voltages (45 and 60 V) and times (30 and 60 min) are presented in Fig. 1(b-e). After MAO process, highly porous structure consisting of micropores could be clearly detected on the surface of samples. This structure which was the conventional morphology of MAO process called micro-arc channels was developed during the micro-discharging time (Yerokhin, Nie, Leyland, Matthews, & Dowey, 1999). These porous constructs consisted of the molten oxide particles randomly distributed on the coating as well as gas bubbles thrown out of the micro-arc discharge channels (Cai et al., 2011). The percentage of the pores on the total oxide surface defined as surface porosity (Tang, Zhao, Jiang, Chen, & Zuo, 2010) as well as the average pore size of coatings were extracted from SEM images and shown in Table. 1. The coatings prepared at lower voltage (45 V) (Fig. 1 (b) and (c)) exhibited a relatively non-uniform surface appearance with small pore size. In this voltage, increasing the time of MAO process from 30 min (45v30m sample) to 60 min (45v60m sample) led to an increase in the average pore size (two-times) and decrease in the average porosity (about 5%), respectively. Moreover, increasing the voltage from 45 V to 60 V noticeably enhanced pore size and reduced porosity (Fig. 1 (d) and (e) and Table 1). According to Fig. 1(d), pores with the sizes of around 3.32±1.97 μm (indicated by arrows) were uniformly covered the surface of sample. Noticeably, the pore size and porosity of 60v60m were about 9.14±4.67 μm and 32% respectively, which were about 10 times greater and the porosity 33 % lower than those of 40v30m. Moreover, compared to the samples prepared at 45 V in which some regions were not coated, the whole surface was completely covered with MAO coating when 60 V was applied. The difference between these morphologies and the distribution of pore size could be ascribed to the different features of micro-sparks such as their size and the number appearing during MAO process. This behavior was similarly reported in previous researches (Ezhilselvi, Nithin, Balaraju, & Subramanian, 2016). Moreover, compared to the SEM images of 60v30m coating, bigger pores with non-uniform size were distributed on the 60v60m sample. In addition, some microcracks (as marked by arrows) could be detected on the surface of 60v60m coatings which might be due to increasing MAO process and the thickness of coatings leading to the formation of cracks or distraction in some points of coatings. These pores and cracks may result in the poor corrosion resistance of the MAO coating during the immersing in the corrosive

environments.

The average surface roughness of samples (Table. 1) also confirmed the formation micro and macropores at MAO coated samples depending on the voltage and time of process. Increasing voltage and time of MAO process enhanced the surface roughness more than 10.5 times from 2.702 ± 0.69 (at 45v30m) to 21.096 ± 2.38 (at 60v60m) due to the formation of micropores and cracks at 60V60m sample. Therefore, it could be concluded that during the MAO process, working voltage revealed the most effective role on the changing the roughness of samples. Therefore, in order to create a uniform layer overlying the substrate, 60 V and 30 min were favorable voltage and time, respectively.

The cross-section morphologies of the MAO coatings prepared at two different voltages and times (45v30m and 60v30m samples) (Fig. 2(a) and (b)) revealed that the MAO coatings included a superficial porous layer with numerous pores and micro-crack and an internal nearly dense layer. This structure was similarly reported by Wang *et al.* (Wang, Wang, Zhang, & Zhang, 2005) who revealed that the compact internal layer was produced during the preliminary discharge sparking time. The superficial porous outer layer could authorize more corrosive medium absorbed into the MAO coatings and reduce the corrosion resistance. The internal nearly dense layer formed a rough wavy interface without any cracks with the substrates suggesting the appropriate adhesion between the coating and the substrate. This tight interface was similarly reported in previous researches in which the formation of sintered interlocking with wonderful bonding strength was suggested between two components (Liang, Hu, & Hao, 2007; Lin et al., 2013; Yerokhin, Leyland, & Matthews, 2002). Additionally, the thickness of 45v30m sample (Fig. 2(a)) was about 300±50 μm which was enhanced to about 500±50 μm at 60v30m sample (Fig. 2 (b)) confirming the efficient role of voltage on the thickness of coatings.

The linear element distribution of 60v30m sample along the line indicated in Fig. 2(b) is shown in Fig. 2(c). EDS analysis of two different points of 60v30m indicated with (1) and (2) are also presented in Fig. 2(d). Results revealed the elements of Mg, Si, O and F were integrated into the coating through MAO reaction confirming the XRD results. Mg concentration progressively reduced from substrate toward the coating, while the Si concentration revealed reverse trend. Furthermore, the alterations of the concentration of F in MAO coating also revealed the gathering of F atoms at the outer part of coating. EDS analysis of two different points also demonstrated that F was incorporated at the outer part of the coating while its content was

relatively low. According to the results of XRD and EDS analysis, while silicate based components such as forsterite was formed in the primarily stage of MAO process followed by MgF_2 formation.

3.2. Electrochemical corrosion evaluation of MAO-treated samples

The corrosion resistance of untreated AZ91 as well as MAO coated samples was assessed through potentiodynamic polarization analysis in PBS solution at ambient temperature (Fig. 3(a)). The consequent polarization parameters consisting of corrosion current density (I_{corr}) and corrosion potential (E_{corr}) as well as corrosion rate (CR) extracted from the graphs by extrapolating the anodic and cathodic branches of the polarization curves were presented in Fig. 3(b). Compared to bare AZ91 substrate, while the corrosion potentials (E_{corr}) of 45v30m, 45v60m and 60v30m were shifted to positively values, it was shifted to negative ones for 60m60v sample. According to previous researches, the E_{corr} of the samples straightly alters based on the comparative greatness between the anodic and cathodic reaction rates, and does not have any relation to the corrosion resistance (Lin et al., 2013). Generally, the corrosion current densities of various MAO coated samples were at least 4.5 times lower than that of bare AZ91 suggesting that MAO coatings have effective role on the corrosion resistivity of AZ91 alloy. Noticeably, while the corrosion current density of the bare AZ91 was 8.01 $\mu A/cm^2$, it reduced to less than 0.37 $\mu A/cm^2$ for 60v30m. Moreover, the corrosion rate of AZ91 alloy significantly reduced after MAO process. Remarkably, the corrosion rate of AZ91 (22.59 mm/year) decreased 21.7 times at 60v30m sample confirming the effective role of MAO process to improvement of the corrosion resistivity.

Similar to the most of previous researches on the MAO treated samples (Guang-Ling Song 2014), the bare Mg based alloy is protected by a thin passive layer mainly consisting of MgO which spontaneously formed on the surface of samples. However, this layer could easily be attacked in aqueous medium leading to weak corrosion resistivity. Our results revealed that MAO process significantly reduced the corrosion current density of AZ91 substrate depending on the working time and voltage. In this regard, at 45 V condition, increasing the time of MAO process from 30 min to 60 min reduced the current density about two times which could be due to the enhanced modification of more surface using ceramic based coatings (Fig. 1) resulted in

enhanced corrosion resistance. Moreover, increasing the voltage from 45 to 60 V significantly reduced current density more than four times due to enhanced thickness of coating (Fig. 2(a and b)). However, due to the formations of pores and microcracks developed at 60v60m treated sample which enhanced the risk of aggressive ions to intrude, the corrosion current density enhanced compared to 60v30m.

According to the previous research, when MAO treated samples were immersed in a corrosive solution, the solution consisting of aggressive ions (e.g. Cl^-) penetrated through structural defects consisting of pores and cracks and ultimately moved to the substrate/coating interface. In this situation, MgO phase formed naturally on the surface of substrate, by exposure with solution started to react with the aggressive solution and changed to $Mg(OH)_2$ leading to the saturation of the pore solution with $Mg(OH)_2$. The formation of OH^-ions or the consumption of H^+ ions induced by the reactions would locally lead to an excess of OH^-ions, thus to a higher pH value and, accelerate the corrosion rate. Therefore, the presence of cracks and pores which resulted in the faster penetration of the corrosive solution to the substrate resulted in the accelerated corrosion (Guang-Ling Song 2014).

EIS analysis was performed in PBS solution and the Nyquist and Bode plots of the samples were evaluated to further study the electrochemical characterization of MAO coatings. Nyquist plots of uncoated and MAO coated AZ91 samples are presented in Fig. 3(c). While all Nyquist plots consisted of one capacitive depressed semicircles, the diameter of this capacitive-arc varied depending on the coating conditions. Similar to other researches (Dan, Hui, Li, & Wu, 2008), the capacitive-arc diameters of all coated samples were much larger than that of uncoated AZ91 sample at high frequency region. The formation of one loop plot might be due to the limited diffusion of PBS in the upper porous layer of MAO. In this condition, due to the barrier role of dense depth layer of MAO coating, PBS could not diffuse in the depth layer of coating. Bode plots of EIS data for bare AZ91 as well as MAO treated samples are shown in Fig. 3(d). Generally, in Bode plots, greater impedance modulus (Z) at lower frequency region indicated better corrosion resistance. The variation in the impedance modulus (Z) with frequency also proposed that the protective layer which formed on the surface of the bare substrates, could be attacked by the electrolyte leading to the comparatively reduced corrosion resistance. According to Fig. 3(d), compared to sampled treated at 45 V, 60v treated samples revealed higher impedance. Moreover, while there was no significant different between the behavior of 45v30m

and 45v60m samples at lower frequency region, 60v30m sample revealed greater impedance modulus (Z) at lower frequency region than 60v60m sample. Based on our results, 60v30m sample with the largest diameter semicircle in nyquist plot and the most impedance in bode plot revealed the best corrosion resistance of these coatings is for this MAO coating. In a similar study, Ezhilselvi et al. (Ezhilselvi et al., 2016) prepared MAO coatings on AZ31B magnesium alloy using alkaline silicate electrolyte at various current densities. Results demonstrated thr significantly improvement of electrochemical properties of MAO coated AZ31B Mg alloy in 3.5% NaCl solution compared to the bare AZ31B Mg alloy. Jiang et al. (Jiang et al., 2013) also confirmed similar resulted on the MAO treated ultra-fine grained AZ91 mg alloy compared the uncoated AZ91. Gu et al. (Y. Gu, Bandopadhyay, Chen, Ning, & Guo, 2013) investigated the long-term corrosion behavior of MAO coated AZ31 Mg alloys immersed in simulated body fluid for 28 days. Results revealed that the corrosion resistance of the coated Mg alloys could be enhanced by the optimizing of the electrolyte concentration, and was improved after immersing the coated samples in simulated body fluid for more than 14 days.

According to our results, 60v30m was the optimized MAO treated sample which was applied for the second coating layer of self-assembled PEI/KC coating.

3.3. Characterization of PEI/KC: MAO-treated AZ91 sample

The surface microstructure of the surface of PEI/KC: MAO-treated AZ91 sample is presented in Fig. 4(a). Compared to the surface microstructure of 60v30m sample (Fig. 1(d)), the micropores and cracks formed during the MAO process was partially covered with two-layer polymer coating (indicated by arrow). According to the SEM images, the pore size and porosity of PEI/KC: MAO-treated AZ91 sample was reduced from 3.32±1.97 μm and 37% to 2.06 ±1.25 μm and 28%, respectively which might be helpful for improvement of corrosion resistivity. In this condition, the surface roughness slightly reduced form 19.276±1.951 μm (for 60v30m sample) to 18.596 ± 0.303 μm and the surface became more uniform. The cross-section images of PEI/KC: MAO-treated AZ91 sample at two different magnifications (Fig. 4(b)) confirmed that PEI/KC coating with thickness of 1.5±0.2 μm was developed on the surface of MAO-treated sample. Moreover, the PEI/KC coating not only covered all surface of MAO treated sample, but also filled the pores formed on the various layers of MAO coating which could be helpful to improve corrosion resistivity.

ATR-FTIR spectrum of PEI/KC: MAO-treated AZ91 sample compared to spectra of PEI and KC polymers (Fig. 4(c)) also confirmed the presence both polymers in the coating layer. According to the chemical structure of PEI, the strong absorption bands at 1633 cm^{-1} (Zhang, Zang, Shi, Yu, & Sheng, 2016), 2969 cm^{-1} and 3332 cm^{-1} (Sahiner, Demirci, Sahiner, & Al-Lohedan, 2015; Taranejoo, Chandrasekaran, Cheng, & Hourigan, 2016) were corresponded to the N-H bond. Moreover, the peaks at 1360 cm^{-1} and 1457 cm^{-1} were related to the C-N and C-C bonds, respectively. In another word, KC consisted of the characteristic peaks of C-O (at 926 cm^{-1}), C-H (at 1381 cm^{-1} and 2973 cm^{-1}) and O-H (at 3369 cm^{-1})(Feng et al., 2016). Compared to the FTIR spectra of PEI and KC, the PEI/KC: MAO-treated sample spectrum consisted of the most of the characteristic peaks of PEI and KC polymers. In this regard, the peaks in the rang of 2960-2980 cm^{-1} indicated the characteristic peaks of C-H and the peaks at 3300 cm^{-1} revealed the characteristic peaks of O-H and N-H.

Adhesion strength between the coatings and the substrate is one of the important factors for coatings which could be determined based on the thickness and dense coating structure (Shi, Niu, Shanshan, Chen, & Li, 2015). The result of tensile test of the MAO and PEI/KC:MAO-treated AZ91 samples (Fig. 4 (d)) showed that while the adhesive strengths of the MAO treated sample was 12.82±1.63 MPa, it was enhanced to 16.13±2.53 MPa at PEI/KC:MAO-treated AZ91 sample. According to the Fig. 4(e)) and (f), the coatings were separated from MAO-treated layer. Therefore, higher strength of PEI/KC:MAO-treated AZ91 sample could be due to the penetration of PEI/KC polymer layer within the pores of the MAO layer via mechanical interlocking leading to the strong interaction between two layers as well as the reduction of pores within MAO layer acted as the initial sites of coating rapture. da Conceicao et al (da Conceicao, Scharnagl, Dietzel, & Kainer, 2011) developed PEI coating on AZ31 alloy and demonstrated the maximum adhesion strength of 6.12 MPa. The significantly greater strength of the present PEI/KC: MAO coating could be due to the mechanical interlocking of polymer coating within MAO coating. Similarly, in another study, the adhesion strength of various polymer coatings consisting of poly (l-lactic acid) (PLLA), poly(caprolactone) (PCL) on magnesium substrate were evaluated(Xu & Yamamoto, 2012). Results revealed that the adhesion strength of coating was in the range of 1.8-4.1 MPa, depending on the polymer type.

3.4. Electrochemical corrosion evaluation of PEI/KC: MAO-treated AZ91 sample

The stimulatory efficiency role of MAO and nanolayer PEI/KC coatings was assessed through the potentiodynamic polarization assay in a PBS solution. Potentiodynamic polarization curve of PEI/KC: MAO-treated AZ91 compared to MAO-treated sample (60v30m) is presented at Fig. 5(a). In order to study the effected of MAO treatment on the electrochemical properties, PEI/KC coating was similarly provided on the untreated AZ91 alloy. The average values of the corrosion current density (I_{corr}) and corrosion potential (E_{corr}) extracted directly from the potentiodynamic polarization curves by the Tafel fit method. Our results confirmed that the corrosion current density significantly reduced (about 8 times) from 0.370 $\mu A/cm^2$ (for MAO treated AZ91) to 0.042 $\mu A/cm^2$ (for PEI/KC: MAO-treated AZ91) and the corrosion potential shifted to the positive direction from -1.22 V to -1.03 V. Moreover, the corrosion current density and corrosion potential of PEI/KC on the untreated AZ91 alloy was 2.462 $\mu A/cm^2$ and -1.09 V, respectively. Our result demonstrated that while MAO treatment was more efficient than self-assembled coating, the combination of MAO and PEI/KC coating revealed the significantly higher electrochemical resistance to localized corrosion than both of MAO and self-assembled treatment, alone. In this regard, PEI/KC layer on MAO coating acted as an obstacle versus corrosive electrolyte, via the inhabitation from the corrosive ion penetration through the pores and cracks and, hence, improvement of the corrosion resistivity of AZ91 alloy.

SEM image of PEI/KC:MAO-treated AZ91 sample after corrosion evolution (Fig. 5(b)) showed that the needle like particles were deposited on the sample. EDS analysis (Fig. 5(c)) was also revealed that these needle-like particles mainly consisted of P, Mg and O according to the Mg based corrosion. This morphology was similarly obtained from the untreated and MAO treated AZ91 alloy (Supporting Fig. S1). Compared to untreated and treated AZ91 alloy, less corrosion product could be observed on the polymer coated AZ91 alloy. Similarly, EDS analysis of the needle like deposition formed on the surface of untreated AZ91 alloy (Supporting Fig. S1) confirmed that these products were the magnesium and sodium phosphates resulted from phosphate in PBS which reacted with substrate. Other researchers also focused on the morphology of corrosion products of magnesium alloys and revealed different morphologies such as rod or plate like deposition. The different in the morphology of corrosion products could be due to the technology of casting and subsequent cold and hot working and impurities in the samples as well as the electrolyte solution. For instance, Jia et al (Jia et al., 2016) revealed the needle like deposition on magnesium alloy during cell culture in DMEM based medium.

Moreover, Feliu et al. (Feliu & Llorente, 2015) similarly studied the chemical composition of the corrosion product layers formed on AZ31 and AZ61 magnesium alloys and revealed this needle shape product on AZ61 alloy

EIS assay was employed to investigate the role of polymer coating on the corrosion resistivity of AZ91 alloy (Fig. 6). According to Fig. 6(a), while both kinds of coatings discovered appropriate corrosion resistance, the diameter of the loop for MAO: PEI/KC treated sample was larger than MAO and PEI/KC coated samples. EIS plots of the samples clearly revealed that the capacitive loop of MAO and PEI/KC became enlarged after formation of PEI/KC: MAO-treated samples suggesting that the corrosion resistance of the coating enhanced by the combination of MAO and polymer coating. It might be due to the stimulatory role of the barrier layers of MAO and polymer coating in the prevention from the corrosive ion transfer to substrate. In order to better understand the corrosion behavior of these coatings, the Bode plots were determined and presented in Fig. 6(b). The Bode plots revealed that the impedance at lower frequencies region, enhanced from 5000 Ω for the MAO-treated and 4500 Ω for PEI/KC treated sample to 22000 Ω for the PEI/KC: MAO-treated sample.

According to these EIS spectra, the equivalent circuits of MAO sample and PEI/KC: MAO-treated samples were extracted from the EIS data to better clarify the corrosion behavior of the MAO and two-layer coatings on the AZ91 alloys (Fig. 6(c)). Generally, the equivalent circuit for the metals with MAO coating and MAO/polymer coating in aqueous solution can be expressed similar to Fig. 6 (c (i and ii)), respectively, which could be related to the corrosion behavior of these coatings in long time soaking, in which corrosive solution could penetrate from pores and cracks to the substrate. These equivalent circuits were composed of two time constants in series with oxide coating impedance and coating/solution impedance. In these models, the Rs and R_p represent for solution resistance on electrode surface and the porous layer resistance of the MAO treated coating paralleled with constant phase element (CPE_p), respectively. Moreover, R_b is the barrier layer resistance of the MAO treated coating in parallel with CPE_b (Xiong et al., 2015) and R_1 is the PEI/KC layer resistance of the coating in parallel with CPE_1. Cui et al. (Cui, Liu, Yang, Li, & Lin, 2015) reported the same equivalent circuits for MAO treated Mg alloy. However, as our electrochemical assay was performed after 2 h immersion in PBS solution, the

EIS spectra indicated that the corrosive solution could not diffuse from coating and arrive to substrate. Therefore, equivalent circuit of our EIS results could be simplified as one time constant without large error (Fig. 6(d)). The EIS parameters summarized in Table 2 has brought out numerous features. The impedance of the electrode/solution interface (Rs) was mainly due to the electrolyte solution at high frequency. Based on the results presented in Table 2, it was found that between various treatment approaches, Rs for PEI/KC: MAO was bigger than two others. Moreover, coating capacitance (CPE) of PEI/KC:MAO treated sample (0.1E-6) was less than that of MAO (0.1E-5) and PEI/KC (0.1E-5) coated samples which might be due to enhanced thickness of the coating. Larger capacitance value for MAO and PEI/KC indicated that more electrolyte solution diffused into the coating compared to the PEI/KC:MAO. Moreover, in agreement with the polarization measurements, the R_1 value for PEI/KC: MAO treated sample (21250 Ω cm^2) was significantly larger than that of for MAO (7800 Ω cm^2) and PEI/KC (7600 Ω cm^2).

Based on our results, compared to the single layer MAO coating, the PEI/KC: MAO coating demonstrated considerably lower corrosion current density and higher charge transfer resistance. In this regard, after polymer coating, the surface of the MAO layer was consistently protected. Therefore, the transportation of corrosive ions such as Cl^- and electrolyte was essentially delayed. Therefore, it can be stated that the PEI/KC: MAO coating provided reasonable corrosion barrier for the AZ91 alloy in the PBS solution and demonstrated the potential of the double layered PEI/KC: MAO coating for biomedical applications.

4. Conclusions

Two conventional coating processes of micro-arc oxidation (MAO) and layer by layer (LBL) self-assembly techniques were successfully applied in order to control the corrosion rate of AZ91 alloy. In this regard, MAO process using silicate-fluoride containing solution resulted in development of ceramic-based coating, while self-assembly approach led to the formation of nanocoating of PEI-KC via dip coating process. The following consequences were obtained:

1. The coating thickness enhanced with increasing voltage and time of MAO process.
2. The MAO coatings with porous surface morphology consisted of mainly Mg_2SiO_4 (Forsterite), MgF_2 and MgO were developed in spite of different applied voltages and times of MAO process.

3. Adhesion strength of the double-layered PEI/KC:MAO coating was significantly higher than that of MAO coating (about 1.3 times) due to the improvement of coating and filling the pores.
4. While MAO treatment approach improved the corrosion resistance of AZ91 alloy, double layered PEI/KC: MAO coating revealed a great potential in the protection of AZ91 alloy in PBS solution via prohibition from corrosive ion transportation.
5. Compared to MAO and PEI/KC coatings, PEI/KC: MAO treated sample revealed larger R_{total} (R_s+R_1) (more than 2.8 times) and less coating capacitance (about 0.1 times) values confirming the potential of the PEI/KC: MAO coating for biomedical applications.

Reference

A.L. Becker, A. P. R. J., F. Caruso, (2010). Peptide nucleic acid films and capsules: assembly and enzymatic degradation. *Macromol. Biosci*, Vol 10 pp 488–495.

A.M. Mansouri, F. S., A.A.L. Zinatizadeh , A. Hemati Azandaryani & M. Pirsaheb, K. S. (2014). Preparation of poly ethyleneimine (PEI))/nano titania (TiO_2) multilayer film on quartz tube by layer-by-layer self-assembly and its applications for petroleum refinery wastewater treatment. *Journal of the Taiwan Institute of Chemical Engineers,* Vol 45, pp 2501–2510.

Agarwal, S., Curtin, J., Duffy, B., & Jaiswal, S. (2016). Biodegradable Magnesium Alloys for Orthopaedic Applications: A Review on Corrosion, Biocompatibility and Surface Modifications. *Materials Science and Engineering: C*.

Ana C. Pinheiro, A. I. B., Mafalda A.C. Quintas, Manuel A. Coimbra, António A. Vicente. (2012). K-carrageenan/chitosan nanolayered coating for controlled release of a model bioactive compound. *Innovative Food Science & Emerging Technologies,* Vol 16, pp 227-232.

Anna Trybała, L. S.-W. s., PiotrWarszyn´ ski. (2009). The effect of anchoring PEI layer on the build-up of polyelectrolyte multilayer films at homogeneous and heterogeneous surfaces. *Colloids and Surfaces A: Physicochem. Eng. Aspects,* Vol 343, pp 127–132.

C., P. (2008). Polyelectrolyte multilayer films: from physico-chemical properties to the control of cellular processes. *Curr Med Chem,* Vol 15, pp 685–697.

Cai, J., Cao, F., Chang, L., Zheng, J., Zhang, J., & Cao, C. (2011). The preparation and corrosion behaviors of MAO coating on AZ91D with rare earth conversion precursor film. *Applied Surface Science*, 257(8), 3804-3811.

Crouzier T, B. T., Picart C. . (2010). Polysaccharide-based polyelectrolyte multilayers. *Curr Opin Colloid Interface Sci*, Vol 15, pp 417–426.

Cui, X.-J., Liu, C.-H., Yang, R.-S., Li, M.-T., & Lin, X.-Z. (2015). Self-sealing micro-arc oxidation coating on AZ91D Mg alloy and its formation mechanism. *Surface and Coatings Technology*, 269, 228-237.

da Conceicao, T. F., Scharnagl, N., Dietzel, W., & Kainer, K. (2011). Corrosion protection of magnesium AZ31 alloy using poly (ether imide)[PEI] coatings prepared by the dip coating method: Influence of solvent and substrate pre-treatment. *Corrosion Science*, 53(1), 338-346.

Dan, D., Hui, W., Li, J.-Z., & Wu, X.-D. (2008). Environmentally friendly anodization on AZ31 magnesium alloy. *Transactions of Nonferrous Metals Society of China*, 18, s380-s384.

Detzel CJ, L. A., Rajagopalan P. (2011). Polyelectrolyte multilayers in tissue engineering. *Tissue Eng Part B: Rev*, Vol 17, pp 101–113.

Dima C., C. M., Alexe P., Dima S. . (2014). "Microencapsulation of essential oil of pimento [Pimentadioica (L) Merr.]by chitosan/k-carrageenan complex coacervation method". *Innovative Food Science and Emerging Technologies,*, Vol.22, , pp. 203–211.

Durdu, S., Aytac, A., & Usta, M. (2011). Characterization and corrosion behavior of ceramic coating on magnesium by micro-arc oxidation. *Journal of Alloys and Compounds*, 509(34), 8601-8606.

Ezhilselvi, V., Nithin, J., Balaraju, J., & Subramanian, S. (2016). The influence of current density on the morphology and corrosion properties of MAO coatings on AZ31B magnesium alloy. *Surface and Coatings Technology*, 288, 221-229.

Fan, X., Xu, J., Wang, Y., Ma, H., Zhao, S., Zhou, X., & Cao, X. (2014). Preparation and corrosion resistance of MAO layer/Yb 2 SiO 5 composite coating on Mg alloy. *Surface and Coatings Technology*, 240, 118-127.

Feliu, S., & Llorente, I. (2015). Corrosion product layers on magnesium alloys AZ31 and AZ61: Surface chemistry and protective ability. *Applied Surface Science*, 347, 736-746.

Feng, W., Feng, S., Tang, K., He, X., Jing, A., & Liang, G. (2016). A novel composite of collagen-Hydroxyapatite/kappa-carrageenan. *Journal of Alloys and Compounds*.

Ferreira, A. R., Alves, V. D., & Coelhoso, I. M. (2016). Polysaccharide-Based Membranes in Food Packaging Applications. *Membranes,* 6(2), 22.

Foerst, J., Vorpahl, M., Engelhardt, M., Koehler, T., Tiroch, K., & Wessely, R. (2013). Evolution of Coronary Stents: From Bare-Metal Stents to Fully Biodegradable, Drug-Eluting Stents. *Combination Products in Therapy*, 3(1-2), 9-24.

Gnedenkov, S., Khrisanfova, O., Zavidnaya, A., Sinebryukhov, S., Egorkin, V., Nistratova, M., . . . Matthews, A. (2010). PEO coatings obtained on an Mg–Mn type alloy under unipolar and bipolar modes in silicate-containing electrolytes. *Surface and Coatings Technology,* 204(14), 2316-2322.

Gu, X., Zheng, W., Cheng, Y., & Zheng, Y. (2009). A study on alkaline heat treated Mg–Ca alloy for the control of the biocorrosion rate. *Acta Biomaterialia,* 5(7), 2790-2799.

Gu XN, Z. Y., Cheng Y, Zhong SP, Xi TF. (2009). In vitro corrosion and biocompatibility of binary magnesium alloys. *Biomaterials,* 30, pp 484–498.

Gu, Y., Bandopadhyay, S., Chen, C.-f., Ning, C., & Guo, Y. (2013). Long-term corrosion inhibition mechanism of microarc oxidation coated AZ31 Mg alloys for biomedical applications. *Materials & Design,* 46, 66-75.

Guang-Ling Song , Z. S. (2014). Corrosion mechanism and evaluation of anodized magnesium alloys. *Corrosion Science,* Vol 85, pp. 126–140.

Guo, H., An, M., Huo, H., Xu, S., & Wu, L. (2006). Microstructure characteristic of ceramic coatings fabricated on magnesium alloys by micro-arc oxidation in alkaline silicate solutions. *Applied Surface Science,* 252(22), 7911-7916.

Hiromoto, S., & Yamamoto, A. (2010). Control of degradation rate of bioabsorbable magnesium by anodization and steam treatment. *Materials Science and Engineering: C,* 30(8), 1085-1093.

Jia, Z., Xiong, P., Shi, Y., Zhou, W., Cheng, Y., Zheng, Y., . . . Wei, S. (2016). Inhibitor encapsulated, self-healable and cytocompatible chitosan multilayer coating on biodegradable Mg alloy: a pH-responsive design. *Journal of Materials Chemistry B,* 4(14), 2498-2511.

Jiang, J., Zhou, Q., Yu, J., Ma, A., Song, D., Lu, F., . . . Chen, J. (2013). Comparative analysis for corrosion resistance of micro-arc oxidation coatings on coarse-grained and ultra-fine grained AZ91D Mg alloy. *Surface and Coatings Technology*, 216, 259-266.

K. Cai, A. R., J. Hao, J. Bossert, K.D. Jandt,. (2005). Polysaccharide-protein surface modification of titanium via a layer-by-layer technique characterization and cell behaviour aspects. *Biomaterials,* Vol 26, pp 5960–5971.

Larkin AL, D. R., Rajagopalan P. (2010). Biocompatible, detachable, and free-standing polyelectrolyte multilayer films. *Biomacromolecules* Vol ;11, pp 2788–2796.

Li, J., Song, Y., Zhang, S., Zhao, C., Zhang, F., Zhang, X., . . . Tang, T. (2010). In vitro responses of human bone marrow stromal cells to a fluoridated hydroxyapatite coated biodegradable Mg–Zn alloy. *Biomaterials,* 31(22), 5782-5788.

Liang, J., Hu, L., & Hao, J. (2007). Characterization of microarc oxidation coatings formed on AM60B magnesium alloy in silicate and phosphate electrolytes. *Applied Surface Science,* 253(10), 4490-4496.

Lin, X., Tan, L., Zhang, Q., Yang, K., Hu, Z., Qiu, J., & Cai, Y. (2013). The in vitro degradation process and biocompatibility of a ZK60 magnesium alloy with a forsterite-containing micro-arc oxidation coating. *Acta Biomaterialia,* 9(10), 8631-8642.

Madona Lien Paul, J. S., Natarajan Chandrasekaran, Amitava Mukherjee. (2014). Preparation and characterization of layer-by-layer coated nano metaloxides-polymer composite film using Taguchi design method for Cr(VI) removal. *Journal of Environmental Chemical Engineering 2,* pp 1937–1946.

P. Bertrand, A. J., A. Laschewsky, R. Legras, . (2000). Ultrathin polymer coatings by complexation of polyelectrolytes at interfaces: suitable materials,. *structure and properties, Macromol. Rapid Commun,* Vol 21, pp 319–348.

Park, S. Y., Lee, B. I., Jung, S. T., & Park, H. J. (2001). Biopolymer composite films based on [kappa]-carrageenan and chitosan. *Materials Research Bulletin,* Vol 36, pp 511–519.

R. Dhamodharan, T. J. M. (1999). Adsorption of alginic acid and chondroitin sulfate-A to amine functionality introduced on polychlorotrifluoroethylene and glass surfaces,. *Macromolecules,* Vol 32, PP 4106–4112.

Rodrigo M. Iost, F. N. C. (2012). Layer-by-layer self-assembly and electrochemistry: Applications in biosensing and bioelectronics. *Biosensors and Bioelectronics,* Vol 31, 1–10.

Rojaee, R., Fathi, M., & Raeissi, K. (2013). Electrophoretic deposition of nanostructured hydroxyapatite coating on AZ91 magnesium alloy implants with different surface treatments. *Applied Surface Science,* 285, 664-673.

Sahiner, N., Demirci, S., Sahiner, M., & Al-Lohedan, H. (2015). The synthesis of desired functional groups on PEI microgel particles for biomedical and environmental applications. *Applied Surface Science,* 354, 380-387.

Salih Durdu, M. U. (2012). Characterization and mechanical properties of coatings on magnesium by micro arc oxidation. *Applied Surface Science,* Vol 261, pp 774– 782.

Shi, P., Niu, B., Shanshan, E., Chen, Y., & Li, Q. (2015). Preparation and characterization of PLA coating and PLA/MAO composite coatings on AZ31 magnesium alloy for improvement of corrosion resistance. *Surface and Coatings Technology,* 262, 26-32.

Shu Y, O. G., Wang L, Zou JC, Li QL. . (2011). Surface modification of titanium with heparin–chitosan multilayers via layer-by-layer self-assembly technique. *Nanomater,* pp 1–8.

Syed, J. A., Lu, H., Tang, S., & Meng, X. (2015). Enhanced corrosion protective PANI-PAA/PEI multilayer composite coatings for 316SS by spin coating technique. *Applied Surface Science,* 325, 160-169.

T.S.N. Sankara Narayanan , I. S. P., Min Ho Lee. (2014). Strategies to improve the corrosion resistance of microarc oxidation (MAO) coated magnesium alloys for degradable implants: Prospects and challenges. *Progress in Materials Science,* 60 1–71.

Tang, Y., Zhao, X., Jiang, K., Chen, J., & Zuo, Y. (2010). The influences of duty cycle on the bonding strength of AZ31B magnesium alloy by microarc oxidation treatment. *Surface and Coatings Technology,* 205(6), 1789-1792.

Taranejoo, S., Chandrasekaran, R., Cheng, W., & Hourigan, K. (2016). Bioreducible PEI-functionalized glycol chitosan: A novel gene vector with reduced cytotoxicity and improved transfection efficiency. *Carbohydrate Polymers,* 153, 160-168.

Wang, Y., Wang, J., Zhang, J., & Zhang, Z. (2005). Characteristics of anodic coatings oxidized to different voltage on AZ91D Mg alloy by micro-arc oxidization technique. *Materials and Corrosion,* 56(2), 88-92.

Witte F, H. N., Vogt C, Cohen S, Kainer KU, Willumeit R, et al. (2008). Degradable biomaterials based on magnesium corrosion. *Curr Opin Solid State Mater Sci,* Vol 12, pp 63–72.

Xin, S.-G., Song, L.-X., Zhao, R.-G., & Hu, X.-F. (2006). Composition and thermal properties of the coating containing mullite and alumina. *Materials chemistry and physics,* 97(1), 132-136.

Xiong, Y., Lu, C., Wang, C., & Song, R. (2015). Degradation behavior of n-MAO/EPD bio-ceramic composite coatings on magnesium alloy in simulated body fluid. *Journal of Alloys and Compounds,* 625, 258-265.

Xu, L., & Yamamoto, A. (2012). Characteristics and cytocompatibility of biodegradable polymer film on magnesium by spin coating. *Colloids and Surfaces B: Biointerfaces,* 93, 67-74.

Xue-Nan GU, S.-S. L., Xiao-Ming LI, and Yu-Bo FAN. (2014). Magnesium based degradable biomaterials: A review. *Front. Mater. Sci. 2014,*, 8, 200–218.

Xue, D., Yun, Y., Schulz, M. J., & Shanov, V. (2011). Corrosion protection of biodegradable magnesium implants using anodization. *Materials Science and Engineering: C,* 31(2), 215-223.

Yerokhin, A., Leyland, A., & Matthews, A. (2002). Kinetic aspects of aluminium titanate layer formation on titanium alloys by plasma electrolytic oxidation. *Applied Surface Science,* 200(1), 172-184.

Yerokhin, A., Nie, X., Leyland, A., Matthews, A., & Dowey, S. (1999). Plasma electrolysis for surface engineering. *Surface and Coatings Technology,* 122(2), 73-93.

Zeng RC, D. W., Witte F, Hort N, Blawert C. . (2008). Progress and challenge for magnesium alloys as biomaterials. *Adv Eng Mater,* Vol 10, 4–13.

Zhang, N., Zang, G.-L., Shi, C., Yu, H.-Q., & Sheng, G.-P. (2016). A novel adsorbent TEMPO-mediated oxidized cellulose nanofibrils modified with PEI: Preparation, characterization, and application for Cu (II) removal. *Journal of hazardous materials,* 316, 11-18.

Figure caption

Fig. 1. (a) XRD patterns of pristine AZ91 alloy as well as MAO coated samples. SEM images of (b) 45v30m, (c) 45v60m, (d) 60v30m and (e) 60v60m coated samples.

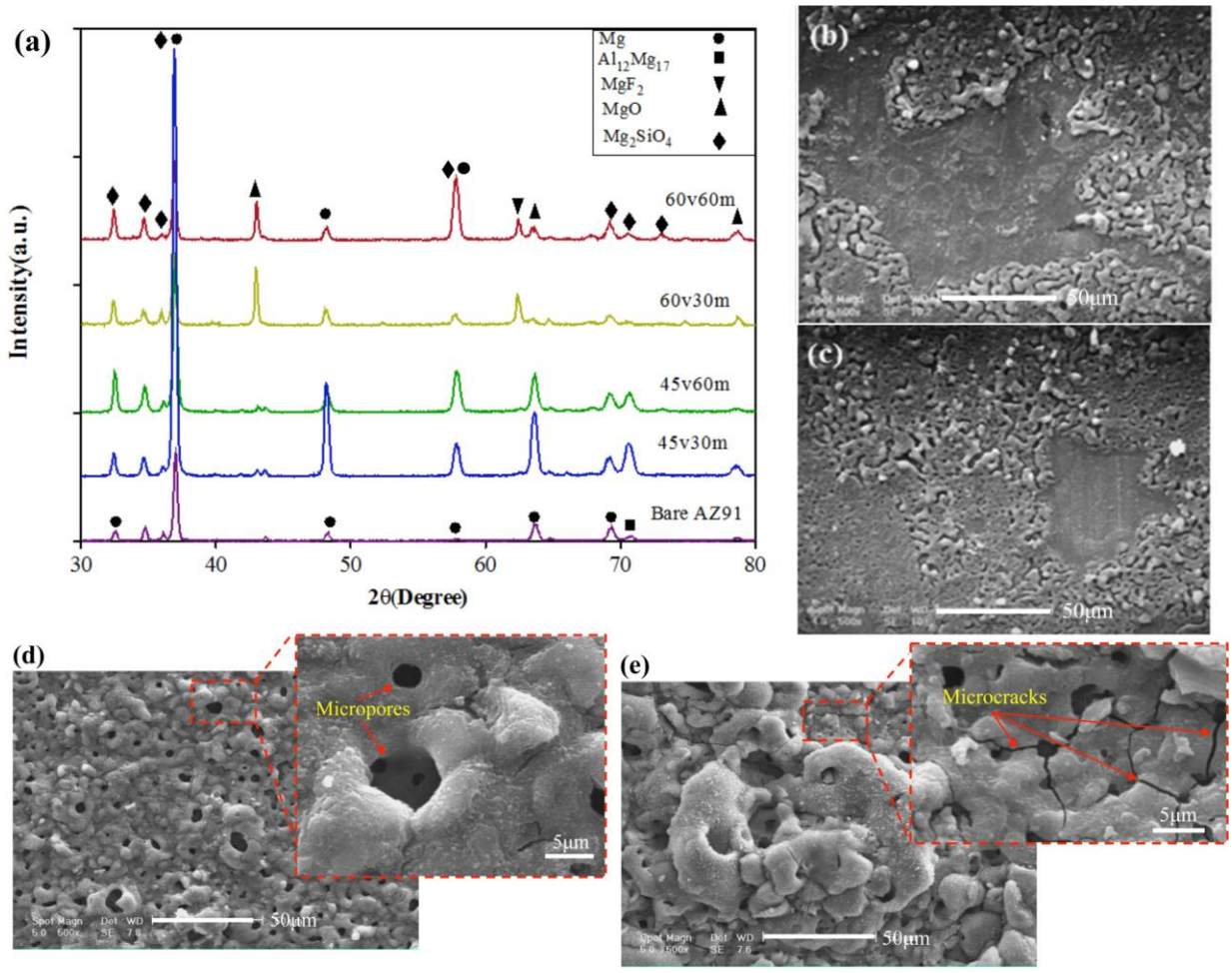

Fig. 2. Cross section morphology of (a) 45v30m (b) 60v30m coatings. (c) EDS linear scanning of "L" line in the cross section of 60v30m coating (b). (d) The EDS spectra and their quantitative results of points "1" and "2" in the cross section of 60v30m coating (b).

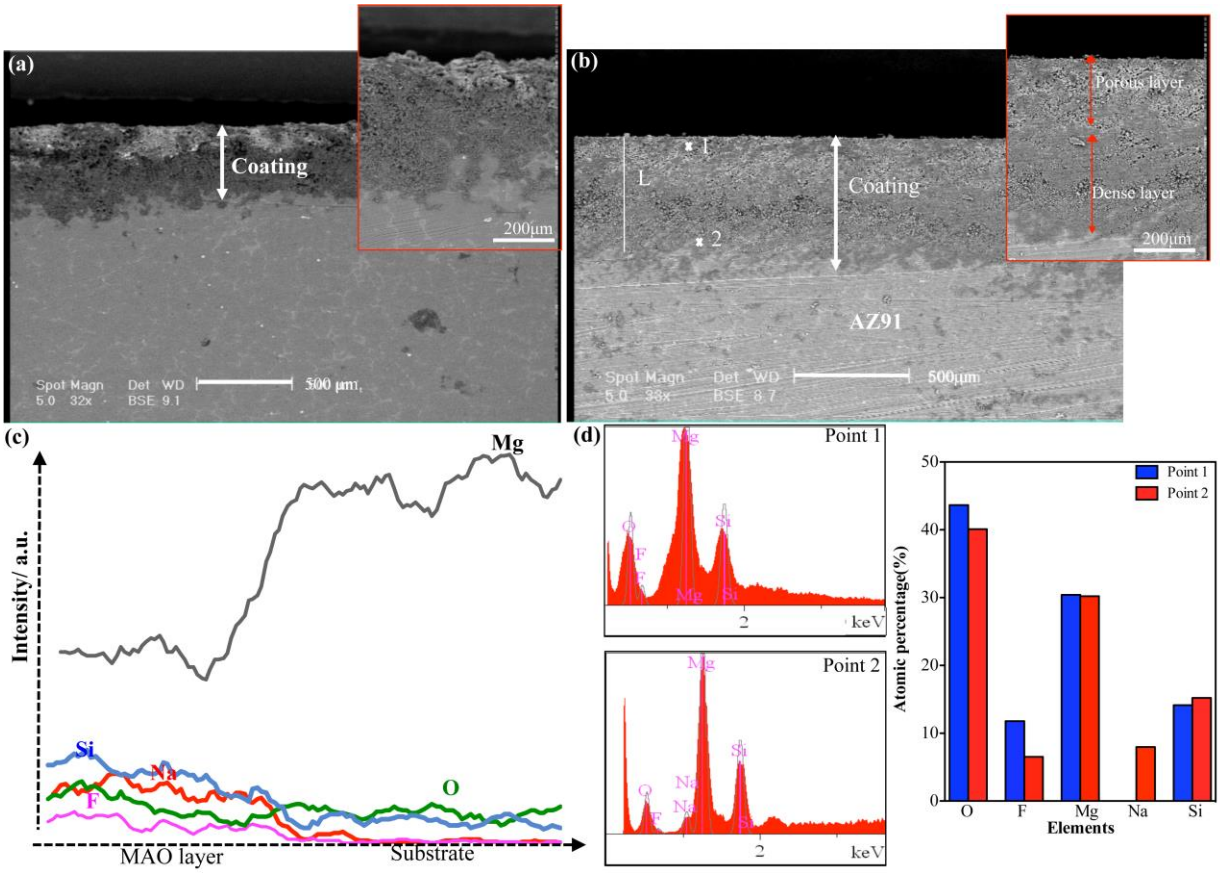

Fig. 3. (a) Electrochemical corrosion polarization curves of MAO treated AZ91 samples and (b) the electrochemical data extracted from potentiodynamic polarization curves in section a. (c) Nyquist plots and d) bode plots of unmodified and MAO treated substrates in PBS.

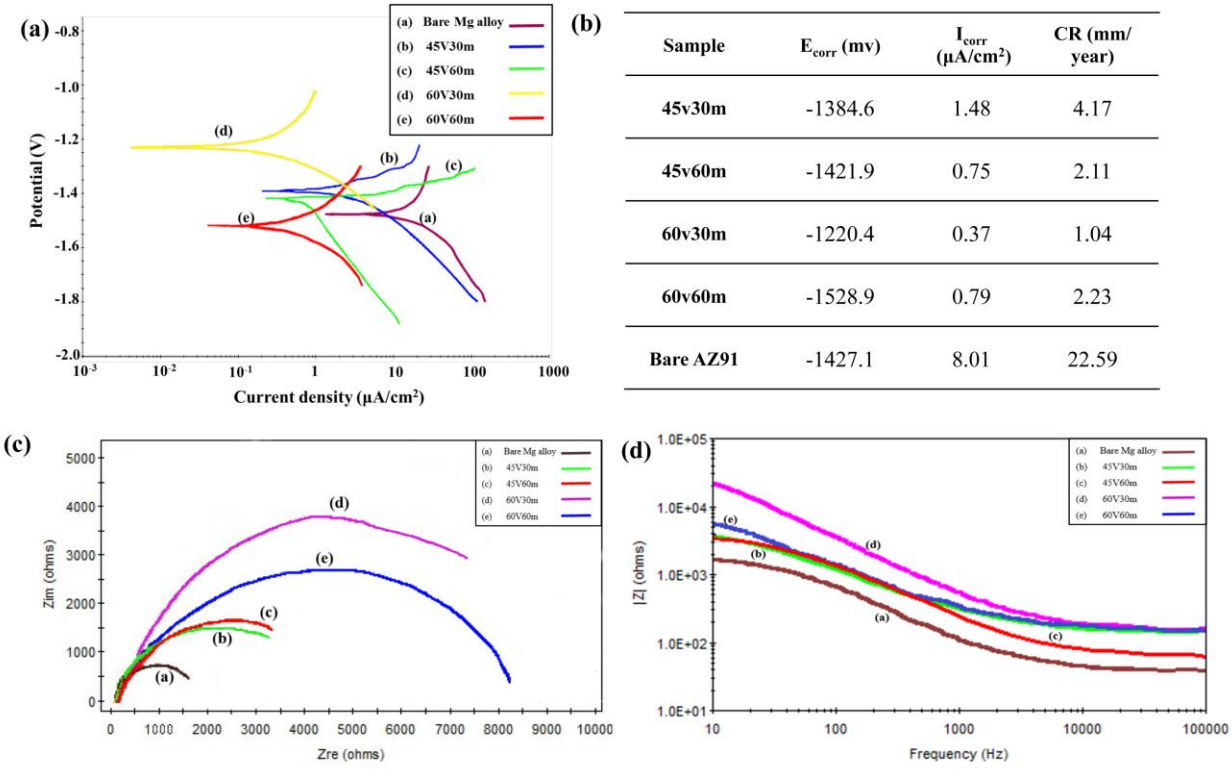

Sample	E_{corr} (mv)	I_{corr} (μA/cm²)	CR (mm/ year)
45v30m	-1384.6	1.48	4.17
45v60m	-1421.9	0.75	2.11
60v30m	-1220.4	0.37	1.04
60v60m	-1528.9	0.79	2.23
Bare AZ91	-1427.1	8.01	22.59

Fig. 4. SEM images of (a) surface morphology and (b) cross section of PEI/KC:MAO coating at two different magnifications. Arrow in the “a” section shows the polymer filled the pore. (c) FTIR spectra of PEI/KC:MAO coating as well as PEI and Kappa Carrageenan powders. (d) Adhesion strength of MAO and PEI/KC:MAO coated sample. The surface macrostructure of (e) PEI/KC:MAO and (f) MAO coated AZ91 alloy after adhesion test

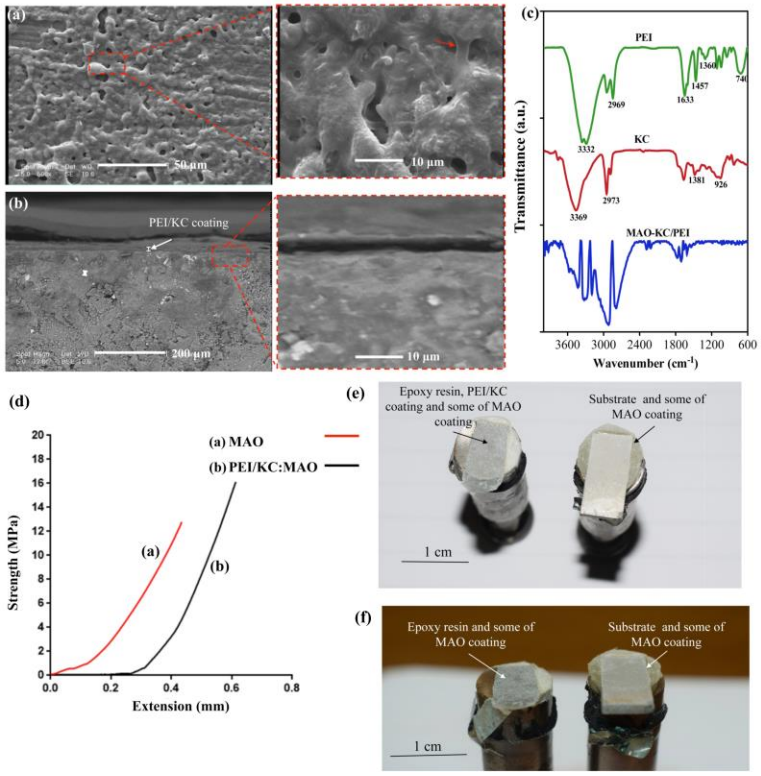

Fig. 5. (a) Typical polarization curves of MAO, PEI/KC and PEI/KC:MAO coated AZ91 samples.(b) SEM images as well as (c) EDS analysis of PEI/KC:MAO coated sample, after electrochemical test.

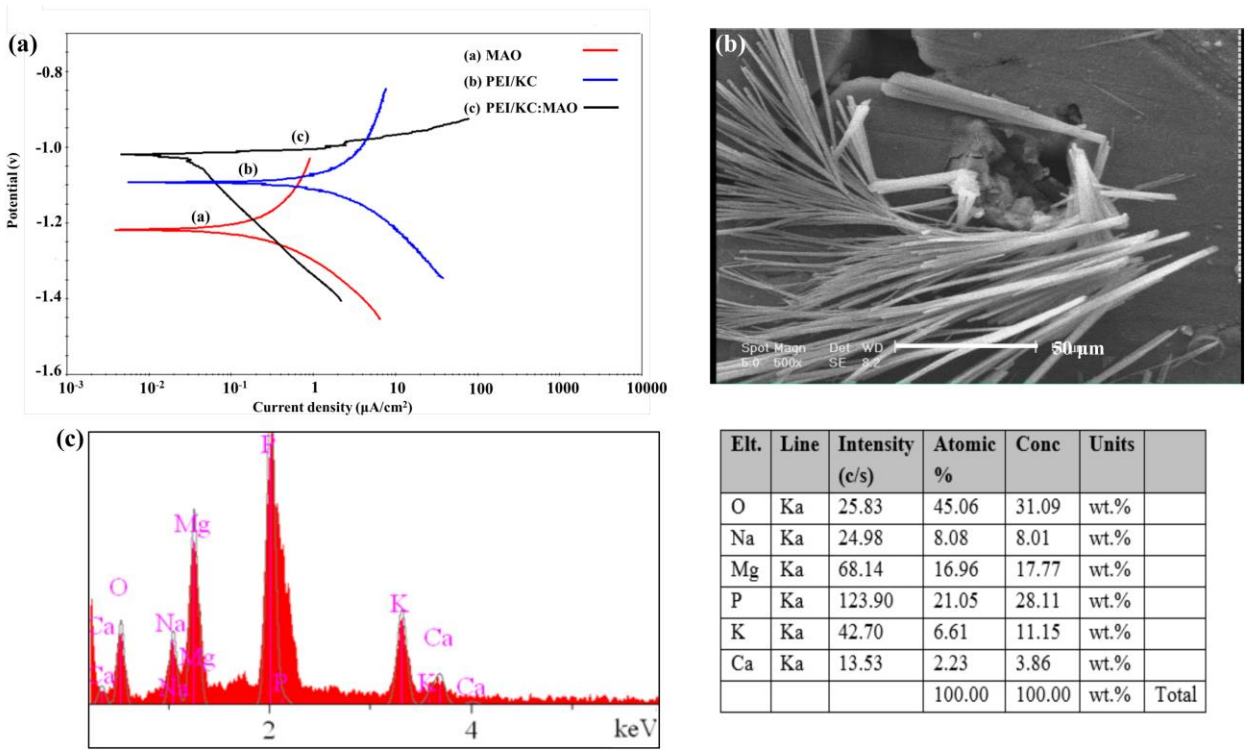

Elt.	Line	Intensity (c/s)	Atomic %	Conc	Units	
O	Ka	25.83	45.06	31.09	wt.%	
Na	Ka	24.98	8.08	8.01	wt.%	
Mg	Ka	68.14	16.96	17.77	wt.%	
P	Ka	123.90	21.05	28.11	wt.%	
K	Ka	42.70	6.61	11.15	wt.%	
Ca	Ka	13.53	2.23	3.86	wt.%	
			100.00	100.00	wt.%	Total

Fig. 6. (a) Nyquist plots and (b) bode plots of MAO, PEI/KC and PEI/KC:MAO coated samples in PBS solution. (c) Electrical equivalent circuits for modeling the behavior of the (i) MAO and (ii) PEI/KC:MAO coated AZ91.(d) the simplified model of coated samples

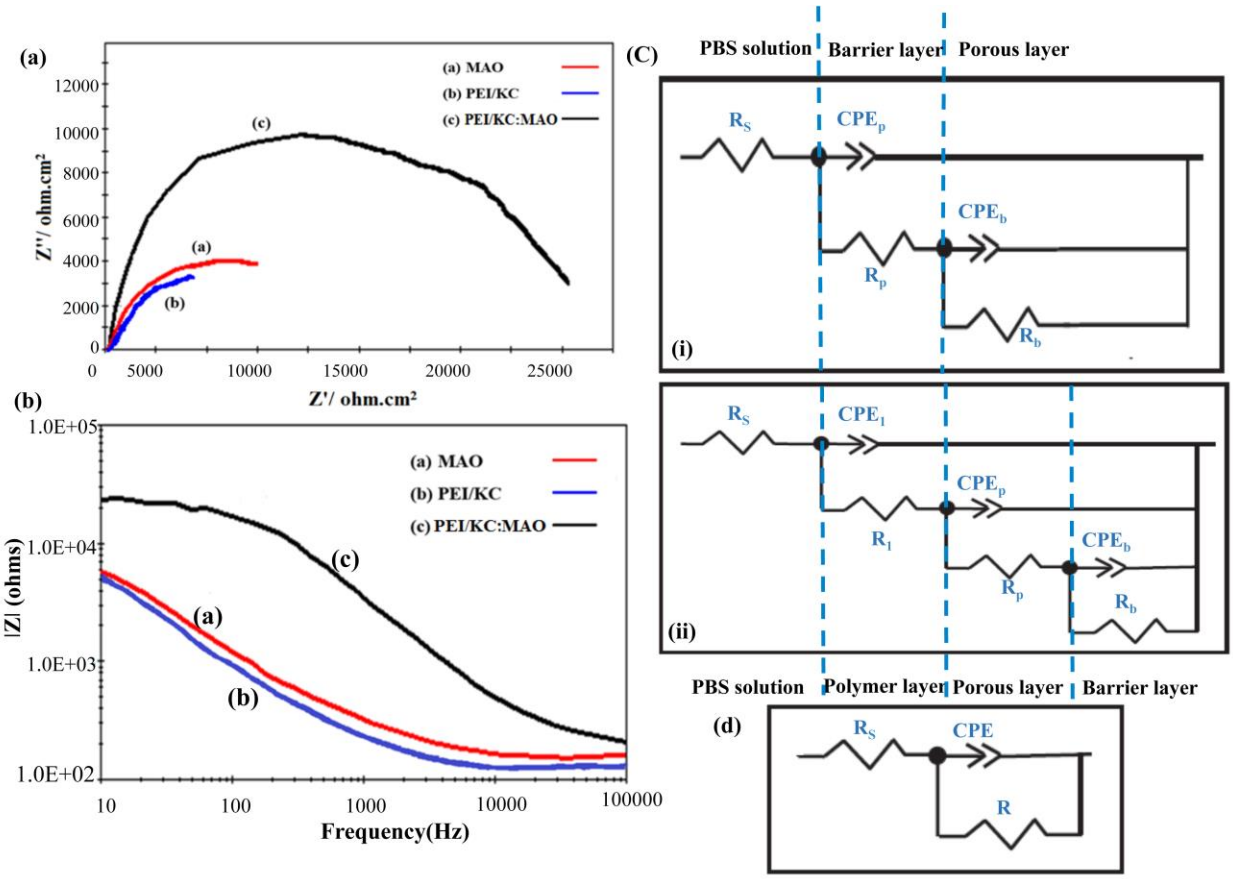

Table 1. The average porosity, pore size and surface roughness of MAO coatings

Sample	**Open porosity (%)**	**Pore size (μm)**	**Roughness (μm)**
AZ91 alloy	-	-	0.328± 0.09
45v30m	65	0.90±0.8	2.702± 0.69
45v60m	50	1.81±0.9	3.706 ± 0.18
60v30m	37	3.32±1.9	19.276 ± 1.95
60v60m	32	9.14±4.7	21.096 ± 2.38

Table 2. EIS data extracted from equivalent circuit (Fig. 6(d)).

Sample	**R_S(Ω cm^2)**	**R_1(Ω cm^2)**	**R_{total} =Rs+R_1**	**CPE (F/cm^2)**
MAO	152	7800	7952	0.1E-5
PEI/KC	90	7600	7690	0.1E-5
PEI/KC: MAO	180	21250	21430	0.1E-6